Impact of control strategies on the degradation of hybrid hydrogen-battery powertrains in railway applications

International Journal of Hydrogen Energy 177 (2025) 151529

Contents lists available at ScienceDirect

International Journal of Hydrogen Energy

journal homepage: www.elsevier.com/locate/he

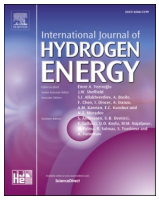

Impact of control strategies on the degradation of hybrid hydrogen-battery powertrains in railway applications

Nicolò Parola, Gabriele Peyrani, Paolo Marocco *, Marta Gandiglio, Massimo Santarelli

Department of Energy, Politecnico di Torino, Corso Duca degli Abruzzi 24, 10129, Torino, Italy

ARTICLE INFO

Keywords:
Hydrogen
Fuel cell
Battery
Degradation
Hybrid powertrain
Railway transport

ABSTRACT

Hybrid hydrogen-battery powertrains represent a promising solution for sustainable transport. In these systems, a fuel cell converts hydrogen into electricity to power the motors and charge a battery, which in turn manages power fluctuations and enables regenerative braking. This study investigates degradation in hybrid powertrain components for the railway sector, focusing on optimizing their operation to enhance durability. The analysis, applied to a real case study on a non-electrified railway line in northern Italy, evaluates different operating strategies by constraining the fuel cell current ramp. The results show that operating the fuel cell with minimal power fluctuations – while relying on the battery to handle power peaks – offers a clear advantage. Specifically, reducing the maximum fuel cell current ramp from 1500 A/s (load-following operation) to 1 A/s (near-constant operation) extends fuel cell lifetime by 50.5 %, though at the expense of a 25.1 % reduction in battery lifetime.

1. Introduction

Railway is currently the most electrified transportation subsector. However, lines with low passenger and freight throughput, where electrification is typically not economically viable, are still serviced by diesel trains. In 2019, direct emissions from the railway sector peaked at 100 Mt of CO_2. According to the IEA models, to align with the NZE (Net Zero Emissions by 2050) scenario, these emissions must be reduced by approximately 5 % annually up to 2030. While electrification is a cost-effective solution for high-traffic lines with few tunnels, its investment costs are normally not competitive for other routes. In such cases, alternative solutions must be explored, with fuel cell hydrogen and battery-electric trains emerging as some of the most promising options [1,2].

Studies and tests conducted since 2005 on various rail application segments [1] have shown that fuel cell hybrid hydrogen-battery trains can satisfy the necessities of rail transportation. Under favorable conditions, especially with low electricity prices, they can become cost-competitive with diesel technology.

Battery-electric trains, in principle, offer a cost-effective and zero-emission alternative to diesel trains. However, they face significant operational constraints, mainly due to battery weight and recharging time. This makes them better suited for services with short daily mileage and requires battery configurations to be specifically tailored to the service requirements, thereby reducing adaptability of the train models [4,5].

To allow fuel cell hybrid hydrogen-battery trains to be widely deployed, the problem of how to maximize the lifetime of both the fuel cell and the battery must be addressed. Since fuel cells are among the primary cost drivers, extending their operating lifespan is a key strategy to reduce overall costs. Similarly, prolonging battery life is crucial, also with the aim of minimizing operational downtime [2].

As of 2017, the cost per km for a fuel cell hydrogen train was calculated to be around 8 €/km, as opposed to 6.5 €/km for diesel trains. However, projections suggested that the cost of the decarbonized alternative could decrease to 6.5–6.8 €/km due to potential reductions in the cost of train procurement, fuel and infrastructure [3]. In Italy, 28 % of the existing railway lines are non-electrified, and for them hydrogen has proved to be among the most viable options, particularly due to its advantages in weight and range [4].

These preliminary remarks highlight the need for a comprehensive analysis of how fuel cells and batteries degrade over the train's operating life.

While numerous studies have proposed models to describe fuel cell degradation, there is still no consensus on the most appropriate approach. Jouin et al. [5] developed a degradation model suited for very

* Corresponding author.
E-mail address: paolo.marocco@polito.it (P. Marocco).

https://doi.org/10.1016/j.ijhydene.2025.151529
Received 26 June 2025; Received in revised form 29 August 2025; Accepted 11 September 2025
Available online 18 September 2025

regular usage profiles of fuel cells, such as constant current or micro-combined heat and power (μ-CHP). Li et al. [6] described the degradation of proton exchange membrane fuel cell (PEMFC) as a function of the thickness of the membrane, highlighting it as the most critical component. They derived various expressions for the membrane thickness as a function of time, with experiments led under constant current conditions, without taking into account dynamic current loads. An approach based on degradation rates dependent on operating conditions was proposed by Desantes et al. [7]. This method allows for the calculation of voltage degradation and was applied to the usage profile of a fuel cell range-extender electric vehicle, making it easily adaptable to railway applications. Similarly, Chen et al. [8] identified the degradation rates associated with the various working currents and, consequently, the lifetime of cells.

The other fundamental point for modeling a hybrid hydrogen-battery train is to know how batteries degrade during their life. In the work by Maheshwari [9], a comprehensive analysis of the degradation phenomena taking place in a lithium-ion battery was presented, distinguishing between calendar aging, which occurs due to the passage of time, and cycle aging, which instead is related to charge throughput. Petit et al. [10] applied a model based on calendar and cycle aging to evaluate the capacity fading of the battery of an electric vehicle that operates with a highly dynamic power demand profile. Few et al. [11] conducted an analysis based on expert opinions regarding the projected improvements in battery lifetime and cost by 2030. They noted that in 2020, the lifetime of batteries was approximately 1800 cycles, and by 2030, it is expected to increase by 67 % if R&D funding remains at current levels.

Concerning the importance of hybridization of the powertrain in the railway sector, Cipek et al. [12] analyzed the opportunity of substituting a common diesel-electric locomotive, operating on a mountainous route, with a hybrid diesel lithium-ion battery alternative. Their study took into account battery degradation in dimensioning the powertrain and showed that hybridization brings a reduction of 15 % in fuel consumption, with slightly worse results when battery aging has taken place. Recent works in the automotive field have explored energy management strategies aimed at minimizing component degradation, using predictive or health-aware control approaches. For example, Jia et al. [13] proposed a degradation-aware hybrid powertrain model, demonstrating the potential of predictive EMS in improving fuel consumption and durability. More recently, Shi et al. [14] proposed a health-aware real-time energy management approach for hybrid fuel cell-battery systems with multiple fuel cell stacks, targeting both system performance and long-term component health.

To our best knowledge, the problem of degradation in hybrid fuel cell-battery systems has never been analyzed in the railway context, and this work wants to take a first look at this topic that could prove decisive for the future of the transportation sector.

1.1. Aim and novelty of the study

The aim of this work is to integrate the study of fuel cell and battery degradation with train hybridization, analyzing their interactions within a railway context. To achieve this, a MATLAB-SIMULINK-based program was developed to evaluate the degradation of the powertrain (fuel cell and battery) in every timestep throughout the train's operating life and assess its impact on fuel consumption.

This analysis is applied to a real case of a hybrid hydrogen-battery train operating on the Brescia-Iseo-Edolo line, a mountainous railway located in northern Italy [15]. The goal is to explore the influence of dynamic constraints on the fuel cell and determine the optimal control strategy for maximizing the lifespan of either the fuel cell or the battery, while also identifying the best trade-off between the two.

The study considers various scenarios among two extreme operating conditions:

- Range extender mode: the fuel cell operates at fixed power to recharge the battery, ensuring that its state of charge never falls below a specified threshold.
- Load following mode: the fuel cell dynamically adjusts its power output based on the instantaneous power demand of the electric motor.

By comparing these strategies, this work seeks to identify the most effective power management approach for enhancing the durability and efficiency of hybrid railway powertrains. The outcomes of this analysis could subsequently support the selection of an optimal control strategy according to a chosen criterion, such as minimizing the total cost of ownership. Nevertheless, such an economic assessment lies beyond the scope of the present study, which instead focuses on the development of a versatile tool for evaluating the degradation of hybrid powertrain components.

To ensure effective use of this tool, it must be customized for each specific powertrain configuration. This involves adjusting numerical parameters related to component sizes, degradation coefficients, and input data that defines the power demands of the fuel cell and battery. Such adaptability allows the tool to be applied to different railway lines and vehicle types, making it a flexible resource for optimizing hybrid train operations.

Overall, the methodological novelty of this study lies in several key aspects:

- Integration of detailed electrochemical and degradation models for both the fuel cell and the battery, allowing for high-fidelity simulation of component behavior.
- Simulation of the entire operative lifetime of the powertrain, enabling analysis of how degradation mechanisms evolve over time and interact with each other as performance progressively declines.
- Application to a real-world railway case study, ensuring relevance and practical value of the results.
- Exploration of a wide spectrum of control strategies by varying the maximum allowable fuel cell current ramp, from load-following to range extender operation, instead of relying on a predefined control logic.
- Flexibility and adaptability of the modeling framework, which can be re-parameterized for different train configurations, service profiles, and route characteristics.

The remainder of the paper is organized as follows. Section 2 briefly introduces the characteristics of the case study. Section 3 describes the modeling approach for fuel cell and battery operation and degradation, along with the train energy management strategy. Section 4 discusses the main results from the analysis of different control strategies. Finally, key conclusions are summarized in Section 5.

2. Case study

The case examined in this work is part of the "H2iseO Hydrogen Valley" project, developed by FNM, FERROVIENORD and Trenord. In its first phase, the project foresees the introduction of six hydrogen hybrid trains, manufactured by Alstom, to operate on the Brescia-Iseo-Edolo railway line [15,16].

The Brescia-Iseo-Edolo railway line is a single track, non-electrified mountain route, 102.7 km long with 31 stops. Brescia station lies at 140 m a.s.l. and Edolo station is at 668 m a.s.l. [17], with a maximum slope of 26 ‰. The maximum permitted speed on the line is 90 km/h, though in some sections it drops to as low as 50 km/h [18]. Traditionally, the service has been operated using diesel multiple units.

The Alstom Coradia Stream H trains offer an autonomy of 600 km, with hydrogen stored at a nominal pressure of 350 bar [19]. Their fuel cells deliver a declared gross power of around 400 kW [20]. In addition, the trains are equipped with batteries, which have a nominal capacity of

about 1000 Ah and a nominal voltage of about 850 V [20]. These batteries can sustain a maximum C-rate of 3C in discharging mode, and −1 C in recharging mode, which are assumed in this study as the battery current limits [21]. The train can reach a maximum speed of 140 km/h [19].

The forward journey must be completed in 176 min [22], followed by a prolonged stop in Edolo, during which the power unit is turned off, and then an equally long return journey. These operating constraints define the train's speed profile, which in turns determines the traction, braking and auxiliary power requirements at each timestep of the journey.

The calculation of the required power (input data for this study) is conducted using a MATLAB-SIMULINK code, referred to in this work as the "train model", which is presented in detail in Ref. [20]. Traction power is supplied by a variable combination of fuel cells and batteries. A key constraint in the model is that the train must start and end its journey in Brescia with the same battery state of charge, as external battery recharging is not foreseen. Despite the constraints on traction power and battery state of charge, it remains possible to regulate the dynamic behavior of the fuel cell. This is achieved by limiting its maximum current ramp, which directly affects how power demand is shared between the fuel cell and battery, as well as the degradation of both components. This regulation is operated by the train model code [20], which takes as input the traction and braking power, the allowed current ramp for the fuel cell and the desired battery state of charge at beginning and end of the journey. Based on these inputs, the code determines the instantaneous power contributions of the fuel cell and battery, which are then used in this study to assess the degradation of both components.

3. Methodology

This section provides a detailed description of the mathematical model developed to simulate the operation and degradation of the powertrain components, namely the fuel cell and the battery.

Fig. 1 illustrates the methodology used to analyze fuel cell operation over time. The main inputs are.

- the polarization curve (I–V curve) of the fuel cell, which evolves as a function of its degradation state
- the power demand, derived from the train model.

These inputs are used to determine the sequence of operating points of the fuel cell throughout a journey. Degradation is then computed based on both the characteristics of each operating point and the variations between successive points. Additionally, hydrogen consumption is calculated at each timestep.

For the battery (Fig. 2), the main difference compared to the fuel cell is that its polarization curve also depends on the state of charge. Furthermore, at each timestep, the calculations determine both the state of charge variation and the battery degradation. The methodology employed to model these processes is detailed in the following sections.

3.1. Fuel cell model

The polarization curve (I–V curve) of the fuel cell is modeled following the approach presented in Ref. [23], explicitly accounting for activation, ohmic and concentration contributions. The full set of equations and input data used for modeling the polarization curve is provided in the Supplementary Material.

The following sub-sections describe the main degradation contributions and the procedure used to update the polarization curve after

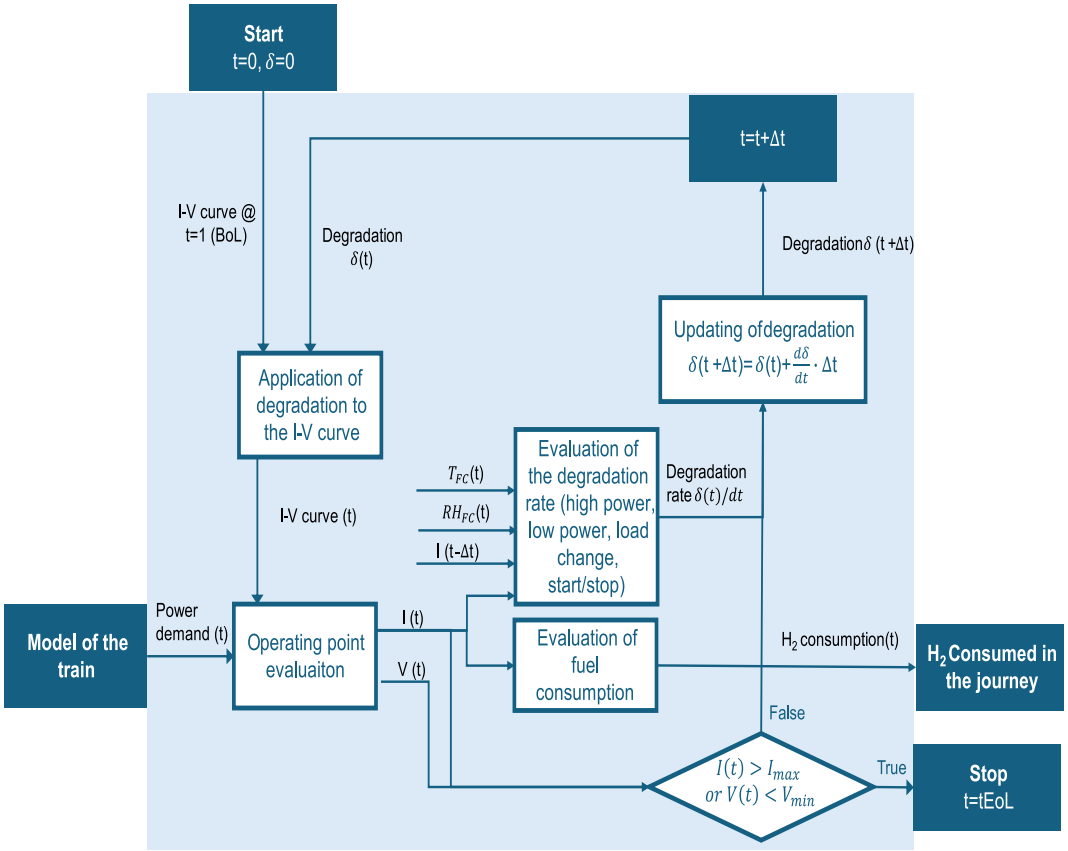

Fig. 1. Schematic representation of the methodology to analyze the fuel cell operation.

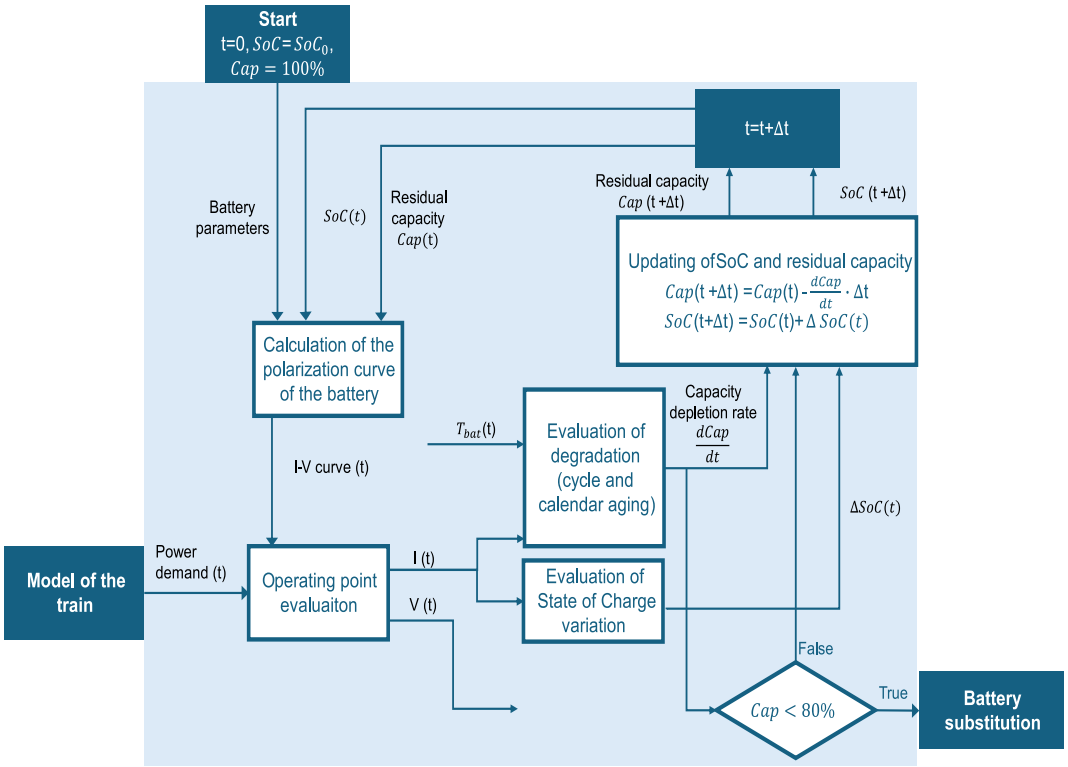

Fig. 2. Schematic representation of the methodology to analyze the battery operation.

degradation is applied. Hereafter, the original, non-degraded polarization curve of the fuel cell will be denoted as $V_0(i_{cell})$.

3.1.1. Degradation of the fuel cell

When the fuel cell is used to supply power, degradation occurs in the form of a voltage loss with respect to the original polarization curve.

To model and quantify the causes of degradation, this work adopts the equations of the event-based model proposed in Ref. [7]. The model distinguishes four sources of degradation for PEMFCs.

- operation at low power
- operation at high power
- load change
- start and stop cycles.

Degradation also depends on the fuel cell operating temperature (T_{FC}, in [K]) and relative humidity ($\overline{RH}$, in [%]). Each contribution is calculated at a given instant as the product of a reference rate, a scaling coefficient (ξ) based on the operating condition (current density i_{cell} or its time derivative $\frac{di_{cell}}{dt}$), and two scaling coefficients (τ and η) related to the environmental conditions (temperature and relative humidity).

All equations composing the model and applied in this work are presented below:

$$\delta = \int_0^t \left[\left.\frac{d\delta}{dt}\right|_{lp} + \left.\frac{d\delta}{dt}\right|_{lc} + \left.\frac{d\delta}{dt}\right|_{hp} \right] dt + \frac{d\delta_{ss}}{dn_{ss}} n_{ss} \tag{1}$$

$$\left.\frac{d\delta}{dt}\right|_{lp} = \left.\frac{d\delta}{dt}\right|_{lp,ref} \cdot \xi_{lp}(i_{cell}) \cdot \tau(T_{FC}) \cdot \eta(\overline{RH}) \tag{2}$$

$$\left.\frac{d\delta}{dt}\right|_{lc} = \left.\frac{d\delta}{dn_{lc}}\right|_{ref} \cdot \xi_{lc}\left(\frac{di_{cell}}{dt}\right) \cdot \tau(T_{FC}) \cdot \eta(\overline{RH}) \tag{3}$$

$$\left.\frac{d\delta}{dt}\right|_{hp} = \left.\frac{d\delta}{dt}\right|_{hp,ref} \cdot \xi_{hp}(i_{cell}) \cdot \tau(T_{FC}) \cdot \eta(\overline{RH}) \tag{4}$$

$$\frac{d\delta_{ss}}{dn_{ss}} = \left.\frac{d\delta_{ss}}{dn_{ss}}\right|_{ref} \tag{5}$$

In the above equations, δ [−] is the coefficient of voltage degradation at a current density of 1 A•cm^{-2}, defined as the ratio between the voltage after degradation and the voltage at beginning of life (BoL) at 1 A•cm^{-2}. It is expressed as:

$$\delta = \frac{V_0(i_{cell}=1) - V(i_{cell}=1)}{V_0(i_{cell}=1)} \tag{6}$$

The subscripts *lp*, *hp*, *lc* and *ss* refer to low power, high power, load change and start/stop, respectively. The first three contributions (*lp*, *hp* and *lc*) are evaluated at each instant of time, integrated over time, and then summed to obtain the overall degradation effect. The fourth contribution (*ss*) is instead added once per start and stop cycle, i.e., whenever the cell is switched off and on again. The coefficients ξ, τ and η account for the operating point, temperature and relative humidity of the fuel cell, respectively. The adopted reference values are provided in the Supplementary Material.

The effect of fuel cell temperature T_{FC} on degradation is represented by the coefficient $\tau(T_{FC})$ [−], defined as follows:

$$\tau(T_{FC}) = -5.390 \cdot 10^{-4} \cdot T_{FC}^2 + 0.399 \cdot T_{FC} - 71.576 \tag{7}$$

The effect of relative humidity $\overline{RH}$ is modeled by $\eta(\overline{RH})$ [−] according to the following expression:

$$\eta(\overline{RH}) = 0.10646 \cdot \exp(0.028 \cdot \overline{RH}) \tag{8}$$

where $\overline{RH}$ is expressed as a percentage. In the analyzed case, the fuel cell is assumed to operate under controlled environmental conditions, with constant values of T_{FC} (333.15 K) and $\overline{RH}$ (80 %). This simplifying assumption can be justified by considering that, given the strong influence of temperature and humidity on fuel cell degradation, railway powertrains are typically equipped with dedicated systems to stabilize these variables. Nevertheless, a more detailed model could account for

temperature and humidity as functions of both ambient conditions and load, thus enabling an assessment of how their variation influences degradation rates.

The parameter ξ [−] is defined differently depending on the degradation contribution. For operation at low power, when $i_{cell} < 0.33$ A•cm^{-2}:

$$\xi_{lp}(i_{cell}) = -0.176 \cdot \ln(i_{cell}) + 0.169 \tag{9}$$

Whereas, for operation at high power, when $i_{cell} \geq 0.33$ A•cm^{-2}:

$$\xi_{hp}(i_{cell}) = \frac{i_{cell}}{i_{hp}} \tag{10}$$

where i_{hp} is equal to 1 A•cm^{-2}, as derived from the calibration of the model. The two conditions are mutually exclusive.

For degradation induced by load change, the coefficient ξ_{lc} depends on the derivative of the current density, which – considering the time discretization Δt – can be expressed as:

$$\xi_{lc}(i_{cell}) = \frac{|\Delta i_{cell}|_{dt}}{2|\Delta i|_{ref}} \tag{11}$$

where $|\Delta i|_{ref}$, equal to 0.99 A•cm^{-2}, is the reference current density change at which the reference voltage degradation is evaluated, while $|\Delta i_{cell}|_{dt}$ is calculated as:

$$|\Delta i_{cell}|_{dt} = \left| \frac{i_{cell}(t) - i_{cell}(t-1)}{\Delta t} \right| \tag{12}$$

Degradation values are calculated at each timestep. At the end of journey j, all degradation contributions over the timesteps of journey j are summed, including the contribution from start and stop, which is counted according to the number of times the cell is switched on and off during journey j. The resulting value is then added to the cumulative degradation from previous journeys (up to journey $j-1$), and a new polarization curve is generated for use in journey $j+1$, following the method described in Section 3.1.2.

3.1.2. Update of the polarization curve of the fuel cell after degradation

Knowing the degradation value of the fuel cell for a generic journey j, the new polarization curve at the end of journey j, which will be used for journey $j+1$, can be evaluated. The formulations adopted to define the updated polarization curve follow the approach presented in Ref. [24].

First, the degradation at 1 A•cm^{-2} is calculated as:

$$\Delta V_{i=1} = \delta \cdot V_O(i_{cell} = 1) \tag{13}$$

Depending on this value, expressed in [V], the degradation of the curve may follow three different behaviors, as reported below:

$$\Delta V(i_{cell}) = \begin{cases} \Delta V_{i=1} \cdot i_{cell}, \Delta V_{i=1} \leq 0.033 \\ 0.033 \cdot i_{cell} + (\Delta V_{i=1} - 0.033), 0.033 < \Delta V_{i=1} \leq 0.066 \\ (\Delta V_{i=1} - 0.033) \cdot i_{cell} + 0.033, \Delta V_{i=1} > 0.066 \end{cases} \tag{14}$$

finally, the updated polarization curve after degradation is determined as:

$$V_{deg}(i_{cell}) = V_0(i_{cell}) - \Delta V(i_{cell}) \tag{15}$$

3.1.3. Identification of the operating point of the fuel cell

The complete fuel cell system is here referred to as a module. The module is composed of n_p stacks in parallel and every stack contains n_s cells in series. At each instant of time t across the train journey, the operating point of the fuel cell module is defined by its current $I_{FC,op}(t)$ [A] and voltage $V_{FC,op}(t)$ [V]. These two values are determined based on the power required from the module $P_{FC,op}(t)$ [W], which is obtained from the train model [20].

To assess the operating point of the fuel cell, it is necessary to know the polarization curve of the fuel cell module. It is defined as the relationship between the stack voltage V_{stack} [V] (which also represents the voltage of the fuel cell module) and the module current I_{mod} [A]:

$$V_{stack} = V_{stack}(I_{mod}) \tag{16}$$

where the module and stack variables are obtained from the characteristics of the single cells as follows:

$$V_{stack}(i_{cell}) = V_{deg}(i_{cell}) \cdot n_s \tag{17}$$

$$I_{mod} = i_{cell} \cdot A_{cell} \cdot n_p \tag{18}$$

where A_{cell} [cm^2] is the single cell area and V_{deg} [V] is the single cell voltage calculated according to Eq. (15). Similarly, the power curve of the fuel cell module represents how the produced power P_{mod} [kW] varies as a function of the current:

$$P_{mod} = P_{mod}(I_{mod}) \tag{19}$$

This equation is obtained from the voltage-current characteristic (polarization curve) of the module:

$$P_{mod}(I_{mod}) = V_{stack}(I_{mod}) \cdot I_{mod} \tag{20}$$

A summary of the main steps to be followed is outlined below.

- The value of $P_{FC,op}(t)$ at a given instant of time t is taken from the train model.
- The power curve (Eq. (19)) is used to identify the value of I_{mod} at which $P_{FC,op}(t) = P_{mod}(I_{mod})$.
- This current value, I_{mod}, is then adopted as the operating current of the module at the instant of time t, i.e. $I_{FC,op}(t) = I_{mod}$.
- The operating voltage of the module at the instant of time t, $V_{FC,op}(t) = V_{stack}(I_{mod})$, is determined by substituting $I_{FC,op}(t)$ in the polarization curve (Eq. (16)).

This fully defines the operating point of the fuel cell module and enables the calculation of the degradation experienced by the fuel cell in the analyzed timestep, which in turn allows to determine the updated cell polarization curve as described in Section 3.1.2. Furthermore, the hydrogen consumption at timestep t ($M_{H2}(t)$ in [kg•s^{-1}]) is also calculated using the Faraday's law:

$$M_{H2}(t) = \frac{I_{FC,op}(t)}{Z \cdot F} \cdot MM_{H_2} \cdot \lambda_{H_2} \tag{21}$$

where Z [−] denotes the number of electrons exchanged during the reaction, F [C•mol^{-1}] is the Faraday constant, MM_{H_2} [kg•mol^{-1}] is the molar mass of the hydrogen molecule and λ_{H_2} [−] represents the excess of hydrogen that is sent to the fuel cell module with respect to the stoichiometric amount needed. By integrating $M_{H2}(t)$ along an entire journey and dividing it by the distance travelled, the hydrogen consumption per kilometer is obtained. This value is useful in evaluating the variation of fuel cell efficiency owing to degradation.

3.2. Battery model

The complete set of equations and input data used to represent the battery polarization curve, based on a 2RC model, is provided in the Supplementary Material. The following sub-sections describe how battery degradation is accounted for and how the operating point is determined at each timestep.

3.2.1. Degradation of the battery

The degradation of a lithium-ion battery over its lifespan can be divided into two main components, cycle aging and calendar aging [9]:

- Calendar aging occurs continuously, as the battery is always storing a certain amount of energy. It depends on the state of charge and the temperature of the battery.
- Cycle aging occurs only when the battery is charged or discharged and depends on the charge throughput and the C-rate.

The damage suffered by the battery results in capacity fade and affects its polarization characteristic. From a physical perspective, these effects are inherently coupled, but not linearly correlated. In this model, a simplification is introduced by assuming a linear dependence between the increase in ohmic resistance (R_0) and the reduction in battery capacity (expressed through the state of health parameter, *SoH*), following the empirical trend reported in Ref. [9]. This approach enables a computationally efficient estimation of the evolving battery polarization behavior without explicitly modeling complex degradation mechanisms.

Concerning calendar aging, the capacity depletion at any instant of time is defined as [10]:

$$\frac{dCap_{loss}^{cal}}{dt} = \left[z_{cal} \cdot B_{cal}(SoC) \cdot \exp\left(-\frac{E_{a,cal}}{R \cdot T} \right) \cdot \left(\frac{Cap_{loss}^{cal}}{B_{cal}(SoC) \cdot \exp\left(-\frac{Ea_{cal}}{R \cdot T} \right)} \right)^{1-\frac{1}{z_{cal}}} \right] \cdot b_5 \cdot b_6 \tag{22}$$

where Cap_{loss}^{cal} [Ah] stands for the loss of capacity due to calendar aging, z_{cal} [−] is a dimensionless constant, $E_{a,cal}$ [J•mol^{-1}] is the activation energy modeling the temperature dependency of aging, R [J•mol^{-1}•K^{-1}] is the molar gas constant, T [K] is the temperature, and $B_{cal}(SoC)$ $\left[\frac{Ah}{s^{z_{cal}}}\right]$ is a pre-exponential term dependent on the battery state of charge (*SoC*).The coefficient b_5 is a rescaling factor that accounts for differences in battery capacity, as the reference coefficients were derived for a 7 Ah battery, whereas the battery under study has a capacity of about 1000 Ah. The coefficient b_6 is a fitting parameter introduced to align the calculated capacity loss with values reported in the literature [25].

Capacity loss due to calendar aging is calculated at each timestep during both train operation and idle periods. The value of B_{cal} is assumed to be constant and equal to $B_{cal}(SoC = 30\%)$ for $SoC < 30$ % and to vary linearly between the known values for $SoC = 30$ %, $SoC = 65$ % and $SoC = 100$ %.

The approach used to model cycle aging is instead taken from Ref. [9]:

$$Cap_{loss}^{cyc} = b_7 \cdot b_8 \cdot \Psi \cdot \sum_k d_k \cdot R_k \tag{23}$$

The *SoC*, ranging from 0 % to 100 %, is divided into 10 intervals. The term k indicates the *SoC* intervals in which charging or discharging occurs. The term d_k is the capacity depletion [Ah• ΔSoC^{-1}] in *SoC* interval k, while R_k is the ΔSoC in interval k. The term Ψ [−] accounts for the effect of the C-rate on cycle aging. According to Ref. [9], Ψ is equal to 0 for C = 0, 1 for C = 1 and 1.3 for C = 2, with linear variation between these values. The coefficient b_7 is a rescaling factor to adjust for the fact that the reference degradation values d_k were obtained for a 2.15 Ah battery, whereas the battery under study has a higher capacity. The coefficient b_8 is a fitting parameter introduced to ensure that the estimated battery lifetime is consistent with more recent findings [11]. The parameters adopted to model the loss of battery capacity from both calendar and cycle aging (i.e., Eq. (22) and Eq. (23)) are reported in the Supplementary Material.

It should be noted that Eq. (23) directly provides the capacity depletion, while the result of Eq. (22) must be multiplied by the timestep duration to yield the same quantity. As shown in Eq. (24), the calendar and cycling degradation occurring at each timestep are summed over the entire journey, and the resulting values, i.e., $Cap_{loss,tot}^{cyc}(j)$ and $Cap_{loss,tot}^{cal}(j)$, are subtracted from $Cap(j)$ to obtain the updated capacity for the following journey. Accordingly, for each journey j, the updated battery capacity for journey $j+1$ is computed as:

$$Cap(j+1) = Cap(j) - Cap_{loss,tot}^{cyc}(j) - Cap_{loss,tot}^{cal}(j) \tag{24}$$

where $Cap_{loss,tot}^{cyc}(j)$ and $Cap_{loss,tot}^{cal}(j)$ [Ah] are the overall capacity losses occurring over journey j. In the following journey, the C-rate and the ΔSoC for each timestep will be calculated using the updated battery capacity. Additionally, after each day, calendar degradation accumulated during stop periods is subtracted.

For each journey j, the residual capacity of the battery is used to define the state of health (*SoH*) parameter:

$$SoH(j) = \frac{Cap(j)}{Cap(j=0)} \tag{25}$$

where $Cap(j=0)$ denotes the initial battery capacity, i.e., at the first journey of the train.

The state of health is needed to determine the end of life of the battery, conventionally defined as the moment in which *SoH* goes below 80 %, as stated by Hosen et al. [26] and Lu et al. [27]. Moreover, capacity depletion affects the polarization curve of the battery, as described in Ref. [9]. To account for this effect, the ohmic resistance R_0 (see the Supplementary Material for additional details) is assumed to increase linearly with *SoH* reduction. Accordingly R_0 is updated for each journey j using the following equation [9]:

$$R_0(j) = R_0(j=0) \cdot [2.013 - 1.013 \cdot SoH(j)] \tag{26}$$

3.2.2. Identification of the operating point of the battery

This section presents the method used to determine the operating point of the battery. The procedure, analogous to that adopted for the fuel cell, consists of the following steps:

- For each timestep t, the power charged into or discharged from the battery, $P_{BT,op}(t)$ [W], is provided as an input from the train model.
- Starting from the polarization curve of the battery $V_{BT}(I_{BT})$, the battery power curve is obtained by multiplying each voltage value V_{BT} across the curve by its corresponding current I_{BT}, yielding $P_{BT}(I_{BT})$ [W].
- The operating point of the battery is computed by interpolating the power curve to find the value of I_{BT} that satisfies $P_{BT} = P_{BT,op}(t)$. This value, denoted as $I_{BT,op}(t)$ [A], is then used to determine the operating voltage $V_{BT,op}(t)$ [V] using the polarization curve.

Once the battery operating point ($I_{BT,op}$ and $V_{BT,op}$) is defined, the C-rate at which the battery is operated (defined as the rate at which a battery charges or discharges relative to its maximum capacity) can be determined, which is required for the calculation of Ψ in Eq. (23).

The amount of charge contained in the battery is updated by adding

or subtracting the charge exchanged during the timestep, as follows:

$$Q_{BT}(t+\Delta t) = Q_{BT}(t) - I_{BT,op}(t)\cdot\Delta t \tag{27}$$

where Q_{BT} [Ah] is the amount of charge stored into the battery, and Δt [h] is the timestep duration. The negative sign before $I_{BT,op}(t)$ follows the adopted sign convention, where the current is negative during battery charging and positive during discharging. The same convention applies to $P_{BT,op}(t)$.

Finally, the values of $SoC(t+\Delta t)$ and $\Delta SoC(t)$ are calculated, as they are needed for battery aging evaluation.

$$SoC(t+\Delta t) = \frac{Q_{BT}(t+\Delta t)}{Cap(j)} \tag{28}$$

$$\Delta SoC(t) = SoC(t+\Delta t) - SoC(t) \tag{29}$$

For each journey j, the battery capacity $Cap(j)$ is updated according to Eq. (24).

3.3. Energy management strategy of the hybrid hydrogen-battery powertrain

The code developed for this analysis takes, at each timestep, the power required from the fuel cell $P_{FC,op}(t)$ [W] and from the battery $P_{BT,op}(t)$ [W], as inputs. These values vary depending on the energy management strategy implemented in the train model [20]. The train model determines how the power demand is distributed between the fuel cell and battery while ensuring that the following condition is met:

$$P_{tract}(t) + P_{aux}(t) + P_{comf}(t) = P_{FC,op}(t) + P_{BT,op}(t) + P_{brk,m}(t) \tag{30}$$

where $P_{tract}(t)$ [W] is the traction power (which is positive in acceleration and negative in deceleration), $P_{aux}(t)$ [W] is the auxiliary power needed to operate the fuel cell and the battery, $P_{comf}(t)$ [W] is the power required to ensure passenger comfort, while $P_{brk,m}(t)$ [W] is the power dissipated by the mechanical brakes. Although these values vary throughout a journey, they remain identical between different journeys.

This formulation leaves $P_{FC,op}(t)$ and $P_{BT,op}(t)$ as the two variables to be determined. The fuel cell operating power $P_{FC,op}(t)$ is limited by a maximum value that depends on the size of the fuel cell, whereas the battery power $P_{BT,op}(t)$ can potentially cover the train's total power demand.

The following additional conditions are imposed:

$$SoC(t=0) = SoC(t=end\ of\ journey) \tag{31}$$

$$\left|I_{FC,op}(t+\Delta t) - I_{FC,op}(t)\right| \leq \Delta I_{FC,max} \tag{32}$$

The first condition enforces charge-sustaining operation of the battery, ensuring that its SoC at the beginning and end of each journey is the same. This condition also accounts for battery degradation, meaning that while the actual charge stored in the battery at the end of each journey may vary, it always corresponds to the same SoC.

The second condition limits the maximum allowable fuel cell current ramp, thereby constraining variations in $P_{FC,op}(t)$. The control strategies investigated in this work differ in the value assigned for $\Delta I_{FC,max}$.

The objective is to ensure that $P_{FC,op}(t)$ remains as close as possible to $P_{tract}(t) + P_{aux} + P_{comf} - P_{brk,m}(t)$ while respecting all the mentioned constraints. The battery power $P_{BT,op}(t)$ is then determined accordingly to maintain the power balance defined in Eq. (30).

3.4. End of life conditions for the fuel cell and battery

To determine when to end the simulation, it is necessary to define an end of life (EoL) condition for the fuel cell. In this work, the EoL condition corresponds to the degradation level at which, in order to supply the required power at any instant during a journey, either the current demand from the fuel cell exceeds 1722 A or the fuel cell voltage falls below 240 V. This limitation arises from the operating range of the power converter between the fuel cell and the train motor, which cannot function outside these bounds.

For the battery, the EoL is conventionally defined as the point at which the state of health (SoH), as given in Eq. (25), drops below 80 %. In the simulation, this corresponds to replacing the battery and resetting its SoH to 100 %.

4. Results

This section presents and discusses the main results of the study. It first introduces the polarization characteristics of the fuel cell and battery (Section 4.1), followed by the analysis of the reference case in Section 4.2 (maximum fuel cell current ramp set to 10 A/s). Finally, a sensitivity analysis on the current ramp is performed to assess the impact of different operating strategies on system performance and degradation (Section 4.3).

4.1. Fuel cell and battery polarization curves

Fig. 3 represents the characteristic curves obtained from the mathematical modeling of the fuel cell and of the battery as described in Section 3. The blue curves correspond to beginning of life (BoL) while the red ones to EoL. It can be observed how the battery polarization curve (Fig. 3a) has a positive and a negative current region, corresponding to the phases of charging and discharging. In both the regions, operation at degraded condition results in lower efficiency, with less power being produced for the same supplied charge and less charge being stored for the same recharged power. Concerning the fuel cell, both the polarization and the power curves are pictured (Fig. 3b and c, respectively). The fuel cell can only supply power, so the current is only positive. In the polarization curve (Fig. 3b), two distinct regions are recognizable: one where the voltage drop is more abrupt due to the activation phenomena, and another where it decreases linearly due to ohmic resistance. The region where concentration overvoltage becomes dominant is not represented, as it occurs at a current level that exceeds the maximum current at which the cell can operate. For the same reason, the maximum power point of the fuel cell is not visible on the power curve. The comparison between the BoL and EoL power curves highlights that, similar to the battery, fuel cell also experiences efficiency loss as degradation increases. This leads to reduced power output for the same current and, consequently, the same hydrogen consumption.

4.2. Base case results

This subsection presents the results of the reference case, in which the maximum fuel cell current ramp is set to 10 A/s.

Fig. 4 illustrates how the state of charge of the battery changes through a single journey. The horizontal axis represents time, expressed in terms of journey timesteps (each corresponding to 10 s). The charge-sustaining mode of operation is evident, as the SoC remains the same at the beginning and end of the journey. The battery discharges during acceleration phases and recharges during braking and station stops. The first half of the journey is uphill, with more discharging phases, while the second half is downhill and is exploited to retake the battery to the target SoC. This influences the chosen size of the battery, which must be enough to guarantee that the charge level never goes below 20 % [28]. Overall, the battery serves as an energy buffer, while all the energy on the train originates from hydrogen as the primary energy vector.

Fig. 5 illustrates the degradation of the fuel cell during the train lifetime, distinguishing four degradation phenomena: start-stop, load change, operation at high power and operation at low power. The horizontal axis represents the number of completed journeys since the beginning of operation. Notably, the accumulation of damage follows a linear trend, maintaining a constant rate throughout the fuel cell's

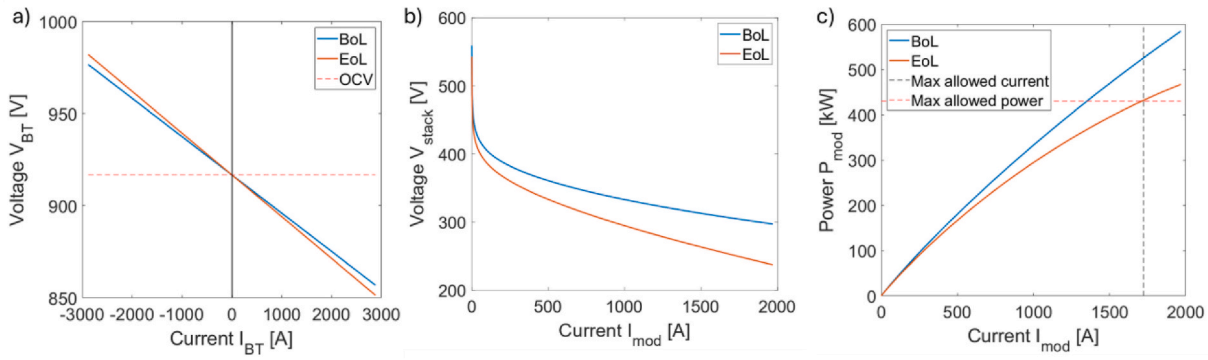

Fig. 3. a) Polarization curve of the battery, b) polarization curve of the fuel cell, and c) power curve of the fuel cell obtained with the implemented model, in blue at BoL and red at EoL. (For interpretation of the references to colour in this figure legend, the reader is referred to the Web version of this article.)

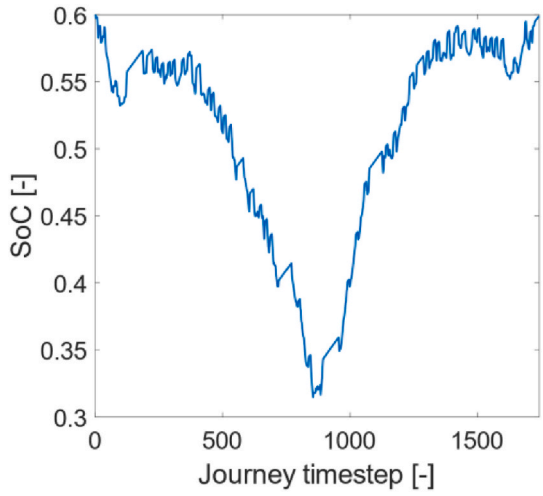

Fig. 4. State of charge (SoC) of the battery during the first forward and backward journey. The horizontal axis represents time, expressed in terms of journey timesteps (each corresponding to 10 s). Results refer to the base case (maximum fuel cell current ramp = 10 A/s).

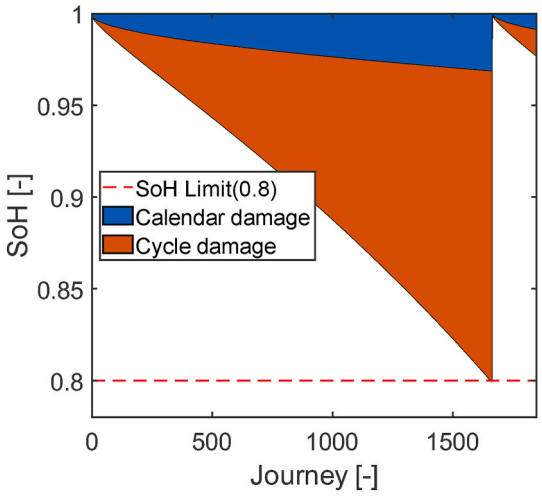

Fig. 6. Loss of battery capacity as the train life progresses distinguished by cause. The results refer to the base case (maximum fuel cell current ramp 10 A/s). The horizontal axis represents the number of completed journeys since the beginning of operation.

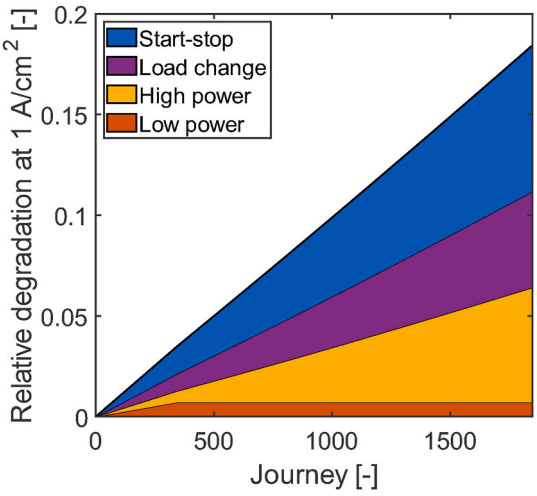

Fig. 5. *Degradation of the fuel cell as the train life progresses, categorized by cause. The results refer to the base case (maximum fuel cell current ramp* 10 A/s*). The horizontal axis represents the number of completed journeys since the beginning of operation.*

lifespan, with start-stop degradation (blue area) being the primary contributor. This suggests that reducing the number of times the fuel cell is switched on and off could be an effective strategy to extend its lifespan. Another notable result is that, after a certain number of journeys, low-power degradation (red area) stabilizes, as the accumulated damage prevents the fuel cell from operating in this low-power region. Consequently, this leads to an increase in the slope of high-power degradation (yellow area).

A similar representation is provided in Fig. 6 for the battery, with damage now expressed as lost capacity. It can be observed that initially the primary contribution of degradation is calendar aging (blue area), which gradually slows as the number of journeys increases. Conversely, cycle aging (red area) accelerates over time, resulting in an overall battery degradation rate that remains nearly constant. However, towards the end of the battery's lifespan, a slight acceleration can be seen, justifying the replacement threshold at 0.8 SoH (battery end-of-life condition) to prevent runaway degradation.

Finally, the evolution of total hydrogen consumption per kilometer can be seen in Fig. 7. The horizontal axis represents the number of completed journeys since the beginning of operation. When compared with Figs. 5 and 6, which illustrate the progressive degradation of the fuel cell and battery, respectively, a clear relationship emerges between components decay (i.e. degradation of fuel cell and battery) and overall fuel consumption. Four distinct regions can be identified in Fig. 7, each corresponding to an increase in hydrogen consumption driven by the

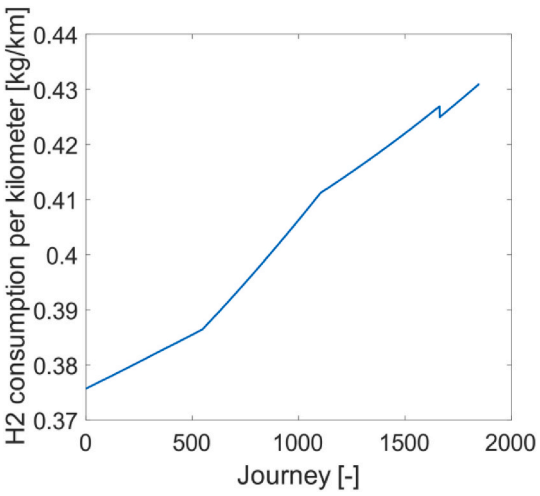

Fig. 7. *Hydrogen consumption* per *kilometer as train life progresses. The results refer to the base case (maximum fuel cell current ramp* 10 A/s*). The horizontal axis represents the number of completed journeys since the beginning of operation.*

progressive loss of performance in the fuel cell and battery. The rate of increase varies across these regions, as described by Eq. (14), which governs degradation. In the first three regions, the different expressions in Eq. (14) determine the slope of the curves. A marked downward step separates the third and fourth regions, corresponding to the replacement of the battery at EoL. At this point, the efficiency of the battery is restored to its BoL value, leading to an immediate reduction in hydrogen consumption before degradation resumes in the new unit.

4.3. Comparative analysis of operating strategies

In the following, the fuel cell ramp rate is systematically varied in order to span the full spectrum of possible control strategies – from the extreme cases of load-following and range extender to a set of intermediate configurations.

The key findings of this assessment are presented in Figs. 8 and 9, which illustrate how different powertrain operating strategies, defined by the maximum allowed fuel cell current ramp, affect the degradation rates of the two components. Specifically, the maximum fuel cell current ramp is varied from 1500 A/s (where the fuel cell handles instantaneous load variations, effectively performing load following) to 1 A/s (where the fuel cell operates as a range extender at nearly constant load, with the battery managing load variations). Results are provided for current ramps of 1, 2, 3, 5, 7, 10, 15, 50 and 1500 A/s. Fuel cell aging is quantified as the voltage loss on the polarization curve per kilometer, while battery aging is measured as capacity loss per kilometer. Although the two extreme current ramp values are unlikely to be adopted in the operation of the real railway case study, they were deliberately selected to frame the full range of possible hybrid powertrain control strategies. The inclusion of intermediate values enables a continuous analysis across the operational spectrum, allowing the results to be generalized beyond any single predefined strategy.

The most immediate observation is the inverse relationship between the optimal conditions for fuel cell and battery longevity: strategies that extend fuel cell life tend to accelerate battery degradation, and vice versa. Comparing the results of Figs. 8 and 9, it can be seen that reducing the maximum fuel cell current ramp from 1500 A/s to 1 A/s decreases the fuel cell degradation rate by approximately 50 %, while the battery degradation rate increases by only about 25 %. This suggests that the gain in fuel cell lifetime outweighs the corresponding reduction in battery durability. Consequently, to enhance the overall durability of the powertrain, it is beneficial to operate the fuel cell as a range extender while relying on the battery to handle instantaneous power demand variations.

An additional important finding concerns the relative contribution of different degradation mechanisms. For the battery, cycle aging is consistently the dominant factor. Instead, for the fuel cell, the primary degradation mechanism depends on the chosen operating strategy: at low allowed fuel cell current ramps, start/stop degradation is the most significant, whereas at high current ramps, load change becomes the main cause of degradation. The relative weight of low- and high-power degradation depends on how the SoC-sustaining constraint (Eq. (31)) interacts with the allowed fuel cell ramp rate. With low ramp limits (range-extender operation), Eq. (30) imposes a higher minimum fuel cell power to close the SoC balance over the journey; the stack therefore avoids the low-power region and accumulates more time at higher current densities, increasing the high-power contribution while decreasing low-power degradation (for ramps <10 A/s, the cell never operates in the low-power range). When the ramp is increased (toward load-following), the required baseline power drops, and the fuel cells follow the power demand, spending more time at low current densities during low-load segments; as a result, the low-power contribution rises, while the high-power contribution declines.

All simulations are performed using the same load profile and assuming that the powertrain is switched off at the end of each journey, reflecting the actual operational practice of the case study. An alternative approach to mitigate start/stop degradation could be to keep the fuel cell idling during the scheduled pauses at Brescia station (the departure and arrival station of the round-trip service) between journeys. However, this would entail additional energy consumption during the idling phase, which must be properly accounted for.

Finally, Table 1 presents the main results, providing a detailed analysis of powertrain degradation across different scenarios. One notable result, not previously discussed, is that the average hydrogen consumption per journey remains practically unchanged (around 83 kg) regardless of the chosen control strategy.

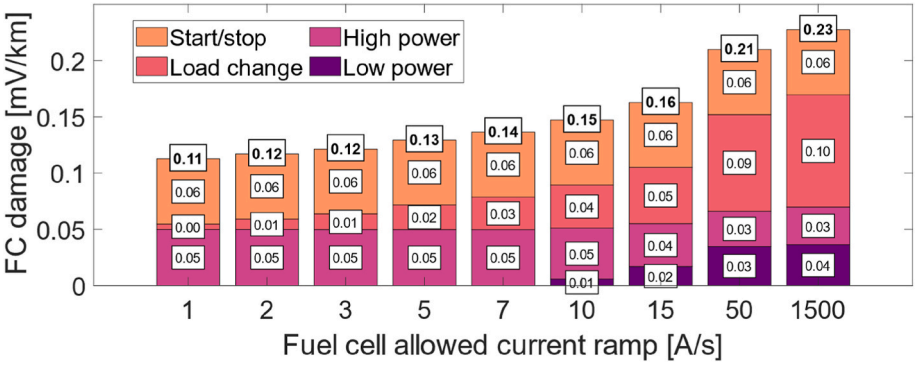

Fig. 8. Damage accumulated per kilometer by the fuel cell for the different operating strategies.

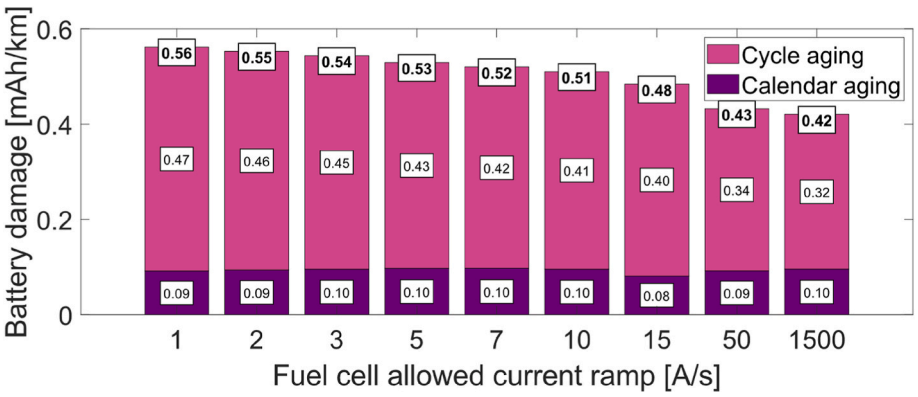

Fig. 9. Damage accumulated per kilometer by the battery for the different operating strategies.

Table 1
Sensitivity analysis for the degradation results with respect to increasing allowed maximum current ramp for the fuel cell (from 1 to 1500 A/s).

Result	1 A/s	5 A/s	10 A/s	50 A/s	1500 A/s
Fuel Cell					
Total operating time [h]	11,706	10,150	8932	6264	5781
Average H_2 consumption $\left[\frac{kg}{journey}\right]$	82.87	82.64	82.66	82.96	83.33
Start-stop degradation contribution	51.3 %	44.6 %	39.3 %	27.5 %	25.4 %
Low-power degradation contribution	0 %	0 %	3.86 %	16.5 %	15.9 %
High-power degradation contribution	44.3 %	38.4 %	31.0 %	15 %	14.7 %
Load change degradation contribution	4.4 %	16.9 %	25.9 %	41 %	44 %
Voltage loss per journey at 1 A cm^{-2} $\left[\frac{V}{journey}\right]$	0.0231	0.0266	0.0302	0.0431	0.0467
Battery					
Battery substitutions	1	1	1	0	0
Calendar aging contribution (1st battery)	14.9 %	15.6 %	16 %	21.2 %[a]	22.7 %[a]
Cycle aging contribution (1st battery)	85.1 %	84.4 %	84 %	78.8 %[a]	77.3 %[a]
Average capacity loss per journey $\left[\frac{Ah}{journey}\right]$	0.1294	0.1210	0.1156	0.1026	0.1007

[a] Battery replacement does not occur during the simulation; therefore, the reported value does not represent the contribution over the full battery lifetime.

4.4. Limitations of the study

Despite the comprehensiveness of the model, some limitations should be acknowledged. The analysis assumes constant environmental conditions such as temperature and humidity. These assumptions were necessary to isolate the effects of degradation and ensure computational feasibility over long-term simulations. That variations in ambient factors would affect the average auxiliary power demand (P_{comf}), thereby increasing or decreasing the overall power required from the fuel cell and its associated degradation. Additionally, abrupt changes in traction (P_{tract}) or braking power ($P_{brk,m}$) – for instance during emergency braking – would alter the dynamic behavior of the power demand, imposing additional stress on the powertrain and accelerating degradation. Under such circumstances, the impact would be more significant on the battery when the fuel cell current ramp is strongly limited.

Additionally, the transient phase of the two resistance-capacitance parallels in the 2RC battery model was neglected due to the adopted 10 s timestep that brings instability in the calculation of the battery voltage (see Supplementary Material). To verify the adequacy of this assumption, comparative simulations were carried out with a finer timestep of 1 s for a limited number of journeys, both including and excluding transients. Results showed only minor differences in key outputs such as battery SoH, hydrogen consumption, and fuel cell degradation. This confirms that neglecting the transients is an acceptable trade-off for the present railway case study, where power demand varies on time scales of tens of seconds. In contrast, for applications with faster load dynamics (e.g., automotive), a finer timestep and explicit modeling of transients would be required.

5. Conclusions

The degradation of fuel cells and batteries plays a critical role in determining the long-term viability of hybrid hydrogen-battery powertrains. This study investigates the impact of different energy management strategies on the lifespan and fuel consumption of these powertrains in railway transport. To achieve this, a MATLAB-SIMULINK model is developed, incorporating degradation models for both the fuel cell and battery components. A key variable examined is the maximum allowed current ramp of the fuel cell, which dictates the powertrain operating strategy. In this analysis, it varies from 1 A/s (range extender mode) to 1500 A/s (load-following mode), with intermediate values representing hybrid approaches.

The proposed methodology is applied to a real case study of a railway line in northern Italy. Results indicate a 50.5 % reduction in fuel cell degradation rate when shifting from the load-following approach (1500 A/s) to the range extender mode (1 A/s), leading to a corresponding increase in the fuel cell's operational lifetime from 5781 to 11,706 h. Conversely, this shift results in a 25.1 % increase in battery degradation rate, reducing the projected battery lifetime from 9212 to 7172 h. The analysis also shows that average hydrogen consumption per journey is practically unaffected by the control strategy, remaining close to 83 kg. This indicates that the reduced efficiency of the battery due to its progressive degradation is offset by a corresponding increase in fuel cell utilization (as journeys progress, battery aging leads to a higher energy demand from the fuel cell, resulting in an upward shift of its minimum operating power level).

Overall, this study suggests that limiting the fuel cell's dynamic behavior to achieve a range extender mode extends its lifespan more

than the corresponding reduction in battery durability. This underscores the greater effectiveness of batteries in handling instantaneous power fluctuations.

Beyond this primary finding, the study also provides useful insights into the relative contributions of different degradation mechanisms and the evolution of the fuel cell and battery polarization characteristics over time. For the battery, cycle aging remains the dominant degradation factor. In contrast, the primary degradation mechanism for the fuel cell depends on the operating strategy: at low allowed current ramps, start/stop cycles cause the most wear, whereas at higher current ramps, degradation is mainly attributed to load changes. These results can help railway operators optimize train operation strategies and make informed decisions about where to focus investments and research in batteries and fuel cells to maximize their lifespan.

Although a full economic assessment is beyond the scope of this work, it is worth noting that the proposed framework can also serve as a foundation for future cost-based analyses. Given that average hydrogen consumption per journey remains nearly constant across all operating strategies, operational costs related to fuel usage can be considered approximately equal. As a result, capital expenditures – primarily associated with component replacements – become the main differentiating factor. Since battery systems are currently much less expensive than fuel cells, adopting a range extender configuration for the fuel cell could also prove advantageous from an economic perspective.

Future developments of this framework will include the integration of a detailed techno-economic perspective, coupling the degradation analysis with cost assessments of component replacement and fuel consumption to identify operating strategies that are both durable and cost-effective. Further improvements may also involve introducing variable environmental conditions to increase model fidelity, using finer time discretization to capture transient dynamics, and incorporating additional operational constraints. Overall, the modeling framework developed in this work provides a solid foundation for these extensions and for the definition of degradation-aware and economically optimized control strategies for hybrid railway powertrains.

CRediT authorship contribution statement

Nicolò Parola: Writing – original draft, Writing – review & editing, Visualization, Validation, Software, Methodology, Investigation, Formal analysis, Data curation, Conceptualization. **Gabriele Peyrani:** Writing – review & editing, Visualization, Validation, Supervision, Software, Resources, Methodology, Investigation, Conceptualization. **Paolo Marocco:** Writing – review & editing, Supervision, Resources, Project administration, Methodology, Investigation, Conceptualization. **Marta Gandiglio:** Writing – review & editing, Supervision, Resources, Project administration, Investigation, Conceptualization. **Massimo Santarelli:** Writing – review & editing, Supervision, Project administration.

Declaration of competing interest

The authors declare that they have no known competing financial interests or personal relationships that could have appeared to influence the work reported in this paper.

Acknowledgements

The case study was developed using the Alstom Coradia Stream H train and the Brescia–Iseo–Edolo railway line as references; however, Alstom and FNM were not involved in this study and have no affiliation with its outcomes.

Appendix A. Supplementary data

Supplementary data to this article can be found online at https://doi.org/10.1016/j.ijhydene.2025.151529.

References

[1] Ruf Y, Zorn T, Akcayoz De Neve P, Andrae P, Erofeeva S, Garrison F. Study on the use of Fuel Cells and Hydrogen in the Railway Environment. Report: State of the art & business case and market potential. 2019 (Accessed 12 September 2025), https://rail-research.europa.eu/publications/study-on-the-use-of-fuel-cells-and-hydrogen-in-the-railway-environment/.

[2] Ruf Y, Zorn T, Akcayoz De Neve P, Andrae P, Erofeeva S, Garrison F. Study on the use of Fuel Cells and Hydrogen in the Railway Environment. Report 3: Overcoming technological and non-technological barriers to widespread use of FCH in rail applications. Recommendations on future R & I. 2019 (Accessed 12 September 2025), https://rail-research.europa.eu/publications/study-on-the-use-of-fuel-cells-and-hydrogen-in-the-railway-environment/.

[3] Ruf Y, Kaufmann M, Lange S, Heieck F, Enders A, Pfister J. Fuel Cells and Hydrogen Applications for Regions and Cities Vol 2. Cost analysis and high-level business case. Sep. 2017 (Accessed 12 September 2025), https://www.rolandberger.com/publications/publication_pdf/roland_berger_fuel_cell_applications_cost_assessment.pdf.

[4] Alstom SA. A growing portfolio of hydrogen traction regional trains [Online]. Available: https://www.alstom.com/press-releases-news/2022/10/growing-portfolio-hydrogen-traction-regional-trains. [Accessed 6 September 2024].

[5] Jouin M, Gouriveau R, Hissel D, Péra MC, Zerhouni N. Degradations analysis and aging modeling for health assessment and prognostics of PEMFC. Reliab Eng Syst Saf Apr. 2016;148:78–95. https://doi.org/10.1016/j.ress.2015.12.003.

[6] Li J, Luo L, Yang Q, Ma R. A new fuel cell degradation model indexed by Proton Exchange membrane thickness derived from polarization curve. IEEE Transactions on Transportation Electrification Dec. 2023;9(4):5061–73. https://doi.org/10.1109/TTE.2022.3188727.

[7] Desantes JM, Novella R, Pla B, Lopez-Juarez M. A modeling framework for predicting the effect of the operating conditions and component sizing on fuel cell degradation and performance for automotive applications. Appl Energy 2022;317 (Jul). https://doi.org/10.1016/j.apenergy.2022.119137.

[8] Chen X, et al. Thermodynamic and economic study of PEMFC stack considering degradation characteristic. Energy Convers Manag May 2021;235. https://doi.org/10.1016/j.enconman.2021.114016.

[9] Maheshwari A. Modelling, aging and optimal operation of lithium-ion batteries. PhD thesis. Politecnico di Torino. Oct. 2018 (Accessed 12 September 2025), https://iris.polito.it/handle/11583/2715622.

[10] Petit M, Prada E, Sauvant-Moynot V. Development of an empirical aging model for Li-ion batteries and application to assess the impact of vehicle-to-grid strategies on battery lifetime. Appl Energy Jun. 2016;172:398–407. https://doi.org/10.1016/j.apenergy.2016.03.119.

[11] Few S, Schmidt O, Offer GJ, Brandon N, Nelson J, Gambhir A. Prospective improvements in cost and cycle life of off-grid lithium-ion battery packs: an analysis informed by expert elicitations. Energy Policy Mar. 2018;114:578–90. https://doi.org/10.1016/j.enpol.2017.12.033.

[12] Cipek M, Pavković D, Kljaić Z, Mlinarić TJ. Assessment of battery-hybrid diesel-electric locomotive fuel savings and emission reduction potentials based on a realistic mountainous rail route. Energy Apr. 2019;173:1154–71. https://doi.org/10.1016/j.energy.2019.02.144.

[13] Jia C, Liu W, He H, Chau KT. Superior energy management for fuel cell vehicles guided by improved DDPG algorithm: integrating driving intention speed prediction and health-aware control. Appl Energy Sep. 2025;394:126195. https://doi.org/10.1016/J.APENERGY.2025.126195.

[14] Shi J, Aarsnes UJF, Tao S, Wang R, Nærheim D, Moura S. Health-aware energy management for multiple stack hydrogen fuel cell and battery hybrid systems. Appl Energy Nov. 2025;397:126257. https://doi.org/10.1016/J.APENERGY.2025.126257.

[15] FNM. H2iseO Hydrogen Valley [Online]. Available: https://www.fnmgroup.it/h2iseo_hydrogen_valley/. [Accessed 6 September 2024].

[16] FNM. Progetto H2iseO. Inquadramento del progetto (Audizione X Commissione). Jun. 2021 (Accessed 12 September 2025), https://www.camera.it/application/xmanager/projects/leg18/attachments/upload_file_doc_acquisiti/pdfs/000/005/837/Memoria_FNM.pdf.

[17] Google Earth Pro 7.3. Geographical information about the brescia-iseo-edolo line [Online]. Available: https://earth.google.com/web/. [Accessed 6 September 2024].

[18] TRANSPLAN. Studio per un nuovo servizio ferroviario della linea Brescia-Edolo (incluso tratto Bornato-Rovato) per trasporto passeggeri. 2022 (Accessed 12 September 2025), https://www.bimvallecamonica.bs.it/scheda-ist/studio-per-un-nuovo-servizio-ferroviario-della-linea-brescia-edolo-incluso-tratto-bornato-rovato-per-trasporto-passeggeri.

[19] Alstom SA. Hydrogen coradia stream product sheet [Online]. Available: https://www.alstom.com/sites/alstom.com/files/2021/09/17/Alstom_Product_Sheet_Hydrogen_Train_EN.pdf. [Accessed 6 September 2024].

[20] Peyrani G, Marocco P, Gandiglio M, Cherchi P, Santarelli M. Techno-economic modeling framework to assess the feasibility of hydrogen-powered trains on non-electrified routes. J Power Sources Oct. 2025;652:237677. https://doi.org/10.1016/J.JPOWSOUR.2025.237677.

[21] Leclanché SA. M3 energy module G/NMC, 65Ah [Online]. Available: https://www.leclanche.com/wp-content/uploads/2021/06/GNMC-65Ah-M3-ENERGY-MODULE.pdf. [Accessed 23 February 2025].

[22] Trenord S.r.l. Linea brescia-iseo-edolo orario [Online]. Available:. https://www.trenord.it/linee-e-orari/circolazione/le-nostre-linee/brescia-iseo-edolo/?code=RE_3; 2024. (Accessed 12 September 2025).

[23] Marocco P, Ferrero D, Lanzini A, Santarelli M. Optimal design of stand-alone solutions based on RES + hydrogen storage feeding off-grid communities. Energy Convers Manag Jun. 2021;238:114147. https://doi.org/10.1016/J.ENCONMAN.2021.114147.
[24] Bezmalinovic D, Simic B, Barbir F. Characterization of PEM fuel cell degradation by polarization change curves. J Power Sources Oct. 2015;294:82–7. https://doi.org/10.1016/J.JPOWSOUR.2015.06.047.
[25] Belt J, Utgikar V, Bloom I. Calendar and PHEV cycle life aging of high-energy, lithium-ion cells containing blended spinel and layered-oxide cathodes. J Power Sources Dec. 2011;196(23):10213–21. https://doi.org/10.1016/j.jpowsour.2011.08.067.
[26] Hosen MS, et al. Twin-model framework development for a comprehensive battery lifetime prediction validated with a realistic driving profile. Energy Sci Eng Nov. 2021;9(11):2191–201. https://doi.org/10.1002/ESE3.973.
[27] Lu L, Han X, Li J, Hua J, Ouyang M. A review on the key issues for lithium-ion battery management in electric vehicles. J Power Sources Mar. 2013;226:272–88. https://doi.org/10.1016/J.JPOWSOUR.2012.10.060.
[28] Kostopoulos ED, Spyropoulos GC, Kaldellis JK. Real-world study for the optimal charging of electric vehicles. Energy Rep Nov. 2020;6:418–26. https://doi.org/10.1016/j.egyr.2019.12.008.